Polarized Dependence of Soft X-ray Absorption Near Edge Structure of ZnO Films Implanted by Yb

Y. Syryanyy (1,2), M. Zając (3), E. Guziewicz (4), W. Wozniak (4), Y. Melikhov (5,6), M. Chernyshova (1), R. Ratajczak (7), and I.N. Demchenko (1,8*)

(1) Institute of Plasma Physics and Laser Microfusion, ul. Hery 23, 01-497 Warsaw, Poland
(2) Institute of Microelectronics and Optoelectronics, Warsaw University of Technology, Koszykowa 75, 00-662 Warsaw, Poland
(3) Solaris National Synchrotron Radiation Centre, ul. Czerwone Maki 98, 30-392 Kraków
(4) Institute of Physics, Polish Academy of Sciences, Lotnikow Alley 32/46, 02-668, Warsaw, Poland
(5) Institute of Fundamental Technological Research, Polish Academy of Sciences, Pawinskiego 5b, 02-106 Warsaw, Poland
(6) School of Engineering, Cardiff University, Cardiff CF24 3AA, United Kingdom
(7) National Centre for Nuclear Research, Andrzeja Soltana 7 Str., 05-400 Otwock, Poland
(8) University of Warsaw, Department of Chemistry, Pasteura 1 Str., 02-093, Warsaw, Poland

(*) corresponding author

PACs numbers: 33.60.Fy 77.55hf 74.25.Jb

Abstract

Virgin and Yb-implanted epitaxial ZnO films grown using atomic layer deposition (ALD) were investigated by X-ray absorption spectroscopy (XAS). XAS study revealed a strong polarization dependence of films determined by the orientation of the polarization vector of the synchrotron radiation to the sample surface. It also indicated that the implantation and subsequent annealing have an important influence on the native point defect complexes in the ZnO. Comparison of experimental spectra with the modelled ones, which are computed based on the linear combination of model spectra corresponding to the selected point defects and their complexes, confirmed the presence of donor-acceptor complexes (mV_{Zn}-nV_O, m=1,4; n=1,2) in the samples under study. The mechanism of vacancy complexes formation is unclear as it takes place under non-equilibrium conditions, for which any theoretical method has not been well established. Exploring the 3d → 4f absorption, it was found that oxidation state of Yb in ZnO is 3+, which is consistent with the XPS findings and previously conducted Resonant Photoemission Spectroscopy (RPES) investigations. The inversion of the polarization dependence for samples with different Yb fluences visible in Yb M_5 spectra can be associated with a tilt of the oxygen pseudo octahedra or/and with their distortion. The analysis of the presented data suggests that the donor-acceptor complexes are present both in as grown and implanted films and may influence their electrical properties. This suggestion was confirmed by previous Hall measurements showing that the resistivity of annealed ZnO:Yb film with a fluence of 5e15 ions/cm^2 decreases by about one order compared to the one with a fluence of 5e14 ions/cm^2.

Introduction

An approach to control and adjusts material properties through creation of defects and/or their agglomerates is currently experiencing a significant interest from researchers out of different disciplines and has led already to advancement in materials design and usage. It is clearly seen, for example, in case of transition metal oxides, where presence of defects significantly alters their electronic structure and chemical properties, which leads to their widespread use in optical and optoelectronic applications. Further efforts in structural design, such as precise manipulation of defects and their qualities, improved control, and fuller understanding of doping and annealing processes, can lead to an improvement of the electrical properties of the host material, provide more active sites, and lead to achievement of superior electrochemical performance. Therefore, improvements in techniques of observations and characterizations of material defects, as well as in understanding of these effects, their influence on materials properties studying and establishing relationships between the structure and properties of materials at the atomic level, researchers can open a new door to the field of materials research.

There are various methods to introduce defects into materials, into zinc oxide that is a subject of this study in particular, with their known advantages and disadvantages. Ion implantation is one of such methods but unluckily, it results in severe damages that degrade the performance of semiconductor devices. Consequently, systematic studies of implantation-induced defects, their interaction with host matrix defects, and efforts to eliminate, manipulate and/or reorganize these defects using annealing are necessary to achieve successful doping through implantation and, as the result, necessary to achieve a good quality material. The ion-implantation effects in zinc oxide have been investigated in a number of works. Some of them are devoted to the study of host matrix and implantation-induced defects [1-3]. To characterize material defects, HRTEM and EELS are often used. Unfortunately, they are limited only to the study of local areas of the material. Positron annihilation spectroscopy (PAS) has emerged recently as a powerful method employed to study defects in semiconductors as it has high sensitivity to vacancy-type defects with detection limit as low as 10^{15} cm^2 [4-7]. This method is quite actively applied to study irradiation induced defects in ZnO with the subsequent comparison with the results from the virgin system. It has been shown that along with of single point defects, like oxygen vacancies and zinc vacancies that are often associated with green/red luminescence, vacancy complexes exist in ion implanted and then annealed ZnO samples. These clusters can be electrically active and may significantly modify the electrical properties of the host matrix. According to [8], from thermodynamic point of view, donor-acceptor clusters are unstable, so, it was suggested that nonequilibrium process associated with an ion implantation and subsequent annealing might be a reason for the vacancies to cluster. Inspired by the work Dong *et al.* [9] and Makkonen *et al.* [6] that were devoted to PAS investigations on metal oxide implanted systems, we decided to test the hypothesis of possible donor-acceptor clustering in Yb implanted zinc oxide using X-ray absorption spectroscopy (XAS) as the main experimental method.

Experimental details

Epitaxial ZnO films (~ 1.5 μm thick) were deposited on a GaN/Al_2O_3 substrate by ALD at 300 °C using a Savannah-100 reactor with diethylzinc and deionized water precursors. Further details of the growth process can be found elsewhere [10]. The crystalline quality of the virgin sample was evaluated by Channeling Rutherford Backscattering Spectrometry (RBS) and High-Resolution X-ray Diffraction (HR XRD). The value of crystalline quality parameter χ_{min} obtained from the RBS/c analysis is equal to 2.8%. HR XRD measurements reveal a sharp and well-defined XRD signal from the ZnO films with the full width at half maximum (FWHM) of the 00.2 reflection evaluated as 0.1055°, while the FWHM of the ZnO -1 to 1.4 reflection evaluated as 0.1491°. The related reciprocal lattice space maps and details of HR XRD experiment have been shown elsewhere [11]. The next step was to implant the ZnO films with Yb ions at room temperature with 150 keV energy and fluence of 5e14 and 5e15 ions/cm^2 using a Balzers MBP 202RP ion implanter at the Institute of Electronic Materials Technology (ITME), Poland. The implanted samples were annealed at 800 °C for 10 min. in oxygen atmosphere using a Rapid Thermal Annealing (RTA) Accu Therm AW-610 system from Allwin Corp.

The X-ray absorption experiments were performed at the Solaris synchrotron, beamline 'PEEM/XAS'. The XANES spectra were obtained recording the total electron yield (TEY) from the samples while scanning the photon energy over the O K-edge and Yb $M_{4,5}$ regions. Since the orientation of crystallites in the film can be obtained from the polarization dependence of the absorption, the X-ray absorption experiments were carried out when polarization vector of synchrotron radiation was oriented along the c-axis (marked "out-of-plane"), perpendicular to sample surface (marked "in plane") and close to "magic" angle. The results obtained for ZnO implanted by Yb films are compared to reference sample of virgin wurtzite ZnO. After normalization to the photon flux the recorded XANES spectra were subject to subtraction of a linear background which was fitted to the flat pre-absorption-edge region. For quantitative comparison the spectra were then normalized to the atomic limit, the range about 100 eV photon energy above the absorption edge, where no angular dependence is observed.

The samples were studied by XPS using a Kratos Ultra Axis spectrometer with monochromatic Al Kα radiation (hν = 1.4866 keV) from an X-ray source with a spot of 700 × 300 μm^2 (due to the analyzer settings in hybrid mode) while operating at 150 W and 15 kV. The high-resolution (HR) XPS spectra were collected with the hemispherical analyzer at the pass energy of 20 eV and the energy step size of 0.1 eV. The photoelectron take-off angle was 45° with respect to the normal to the sample's surface plane. An analyzer acceptance angle was ±7°. No charge compensation was applied. Samples were mounted on the grounded holder. Binding energies (BEs) of the photoelectrons were calibrated using the Au $4f_{7/2}$ photoelectron peak at 84 eV. Selected samples were sputtered using the Ar^+ ion source operating with the 0.5 kV Ar^+ beam energy and the incident Ar^+ ion beam axis of 35◦ to the surface plane. The sputter rate of the ZnO:Yb material was not established.

Results and Discussion

O K edge: allowed transitions and polarization dependence

Figure 1 shows the O *K-edge* XANES spectra of virgin and Yb-doped ZnO films (with dose of 5e14 and 5e15 atoms/cm^2, respectively) recorded at near-normal, near-grazing incidence and close to "magic" angle (when the absorption cross section becomes independent of the orbital orientation). The spectra reveal a strong polarization dependence, see **Figure 1a)**. In samples with cubic symmetry, powders, amorphous, or polycrystalline ones with random orientation of crystallites an angular dependence is not observed. Obtained results manifest preferred orientation of crystallites, along film growth direction, in presented here virgin and implanted ZnO films. For O *K* edge, according to dipole selection rules, the allowed transitions in hexagonal materials are from the initial O 1*s* state of a_1 symmetry to final O *p* states, i.e. $1a_1 \rightarrow a^*_1$ and $1a_1 \rightarrow e^*_1$ [16,12]. The e^*_1 final state results from mixing of p_x and p_y atomic orbitals and will be strongest when the polarization of incoming photons is parallel to the (*x,y*) plane, i.e. for normal incidence (marked "in plane" in **Figures**). Whereas, the a^*_1 state results from mixing of *s* and p_z atomic orbitals can be considered as electronic charge distribution along the *z*-axis. This state will be strongest if the polarization of incoming photons is parallel to *z*-axis, i.e. for grazing incidence in c-plane of w-ZnO (marked "out-of-plane" in **Figure 1**). Consequently, the peaks marked as 1, 2, 4 and 7 shown in **Figure 1a)** correspond to transitions to (p_x, p_y) plane orbitals while 3, 5, 6 and 8 to final mixed s and p_z orbitals. The difference spectrum (spectrum of virgin ZnO film recorded at normal geometry subtracted from that recorded at grazing geometry) is also shown at the bottom of **Figure 1a)**. Similar angular dependence has been observed in ZnO microrod arrays [13] and ZnO:Co thin films [14]. Our calculation of density of states for w-ZnO (see **Figure 1b)**) using FDMNES code [15] agrees with previous reports. As it was mentioned above, the experimental findings suggest a strong correlation between the electronic structure and the geometrical structure in all studied systems: the crystalline virgin ZnO and implanted by Yb ions (latter after post-implantation annealing procedure). The calculated unoccupied partial density of ZnO states shown in [13] agree with our own and suggests that region up to ~538.6 eV indicates a strong hybridization of the Zn 4*s* with the O 2*p* states. In the region 10-20 eV above the absorption threshold the Zn 4*p*-hybridized with the O 2*p* states become dominant. Finally, the contribution from the Zn 3*d* becomes significant in the region above 550 eV, where hybridization of both the Zn 4*p* and the Zn 3*d* with the O 2*p* states is observed.

The TEY technique has a probing depth which is determined by the range of the detected electrons. The primary Auger electrons lose their energy in collisions with valence electrons, producing a cascade of electrons with lower energies. The yield at the surface consists therefore mainly of electrons with a kinetic energy less than 5 eV [16]. Depending on their energy, the escape depth of the Auger electrons lies between ~10 nm in the *soft x-ray range* and ~100 nm *at a few keV* [17-20]. Therefore, electron yield in the soft x-ray range is quite surface sensitive, necessitating the use of ultra-high vacuum. We have to recall also, that in the soft x-ray range fluorescence yields are low, making electron yield the method of choice. Consequently, measurements in TEY detection mode of the O *K-edge* XANES spectra have

been performed using so call “surface” detection mode. Note that due to current limitations at the beamline, there is no possibility to measure “bulk” signal using TFY detection mode. As a result, here we stress that point defects weights calculated below (see **Table 1**) correspond to the sample surface region and may not be the same deeper into the film.

Note a rather delicate modification of the polarization dependence observed between virgin (non-implanted) and implanted by Yb ions ZnO thin films shown in **Figure 1c)**. In this figure, three samples are compared (i.e., before and after implantation with the subsequent annealing) for the selected orientation between the polarization vector of the synchrotron radiation beam and the sample surface, as described above. The observed variation of the unoccupied oxygen *p* states cannot be associated with the contribution of the ytterbium ions, since their concentration in the measured samples is low (below 1.5 at. % according to our XPS investigations). The latter makes it impossible to distinguish this defect from the oxygen side (O K edge) since the host matrix contains a huge number of oxygen atoms (in case of ideal stoichiometry 50:50 (Zn:O)) among which only a minor part can interact with the implanted ion. In other words, it is below the sensitivity limit of the used technique. Consequently, the visible changes of the XANES O *K* edge spectra presented in **Figure 1c)**, are associated with the intrinsic defects of the ZnO matrix and the defects obtained as a result of implantation process.

It should be stressed that the nature of defects in ZnO is extremely complex. Native point defects in this material have been extensively studied as they were expected to determine electrical conductivity that was reported to range from resistive to highly conductive even without any external doping. As theoretical calculation showed, native point defects are either deep (like V_{Zn} or V_O) or have high formation energies (like Zn_O or Zn_i), the presence of native point defects themselves could not explain a high conductivity of undoped ZnO. According to theoretical and experimental studies performed in the last few years, the complexes/clusters of native point defects play an important role in conductivity of this material. Such complexes may involve interstitial zinc (Zn_i), zinc vacancy (V_{Zn}), interstitial oxygen (O_i), and oxygen vacancy (V_O) in different configurations. It was also shown that quite complicated vacancy complexes with a large radius (4 or more Zn vacancies) are needed to explain the results of implantation and irradiation phenomena in ZnO [6]. The existence and subsequent possibility of separation of isolated defects from their complexes using XAS is the subject of present research. The latter, in turn, will allow to confirm or refuting the statement concerning existence of donor-acceptor complexes in implanted and annealed samples proposed by PAS investigations [6, 9]. Taking above considerations into account, a wide spectrum of intrinsic point defects and their complexes was theoretically analyzed using a Green’s function methodology implemented within the software package FEFF9 to deal with polarization dependence.

Simulations of XANES Spectra: usage of meta-models

In order to address the complexity of the problem, the automated program was created, in which the theoretical spectra of all selected models were used utilizing a linear combination in order to obtain the

best agreement between theory and experiment. Such linear combination of several theoretical spectra was called *meta-models*, and the following models were considered for their creation: ZnO-pure, created in host matrix V_{Zn}, V_O, Zn_{oct}, and complexes V_{Zn}-V_O, V_{Zn}-$2V_O$, V_{Zn}-$3V_O$, Zn_{oct}-V_O, $2V_{Zn}$-V_O, $3V_{Zn}$-V_O, $4V_{Zn}$-V_O. Here, interstitial Zn_{oct}, i.e. an interstitial Zn_i atom in an octahedral site, is considered only, as Janotti et al. [21] showed in a comprehensive first-principles investigation of native point defects in ZnO based on density functional theory within the local density approximation (LDA) as well as the LDA+U approach that the octahedral site is the stable site for interstitial metal atom as opposed to the tetrahedral one. A computer algorithm to find the optimal linear combination of several considered models is based on two main parts. In the first part, all possible *meta-models* are created from the selected models list mentioned above, and each *meta-model* is assigned a unique hashtag for quick search and access in future stages of the calculation avoiding duplicate entries. The *length* of necessary *meta-models* needed to obtain a better agreement between theory and experiment was tested (see **Scheme 1** in SuppMat). It turned out that an increase in the *length* of meta-models above 6 does not change the result of the minimalization procedure. After the first part is finished, the algorithm creates several groups, each of which corresponds to a specified measurement angle between the polarization vector of the X-ray beam and the sample surface for a particular experiment. In our case, these are 3 groups with the following Miller indexes: "1 0 0" corresponds to 0° angle marked as “in plane”, “1 0 1” corresponds to 45° marked as "close to magic angle", and "0.2679 0 1" that corresponds to 75° marked as “out-of-plane” in **Figure 1d)**. Note that all described angles are related to the surface of the host matrix. Finally, the second part of the algorithm searches for the optimal weighting factors to minimize the value of the sum of the *R-factor* (marked R_f in the **Table 1**) for all selected groups. The group *R-factor* is calculated between the experimental spectrum and the spectra composed of the linear combination of spectra for each model in the *meta-model* and weighting factors. The sum of the weighting factors for each *meta-model* is normalized to 1. The *differential evolution* routine [22] was used as a minimization procedure during calculation of the optimal weighting factors. The advantage of the algorithm lies in the requirement that the fitting procedure is applied to all selected groups and therefore, it has to satisfy every polarization angle. This increases the probability that the identified *meta-model* can describe the actual sample in the performed experiment. **Table 1** presents the identified *meta-model* with the weights for each of the constituent models with specified defects and/or complexes. Obtained XANES spectra using a linear combination routine are shown in **Figures 1b, d)**.

Identification of existing defects and their complexes and agglomerations

As can be seen in **Table 1**, numerical calculations based on XANES results show that implantation treatment leads to a dramatic change in concentration of particular native defects and their complexes in ZnO films. Let us emphasize that a linear combination of selected spectra, which allows us to estimate the "weights" of the considered phases (models) in the experimental spectrum presented in **Table 1**, generally, can be used to calculate the atomic percentage of the *isolated*

defects, but only if the total percentage of considered defects in the sample/s is known. Since in our case we have a combination of isolated defects and their complexes, only a qualitative description of what is happening can be given.

From this point of view, from **Table 1**, it is possible to see that oxygen vacancy, which is not detected in the virgin ZnO film, clearly appears in both Yb implanted layers. In turn, concentration of Zn_i gradually decreases after subsequent implantation and subsequent annealing processes. We cannot rule out that an insignificant fraction of interstitial zinc or ytterbium atoms after annealing treatment fill the zinc vacancies. However, it should be noted that this fraction is indeed an insignificant one, since the contribution of interstitial zinc atoms after implantation by ytterbium ions and subsequent annealing is lower just by about 11(18)% for samples with fluence 5e14 (5e15) at/cm^2 compared to the virgin sample, respectively (see **Table 1**). It is noticeable that zinc vacancy, V_{Zn}, present in the virgin sample is not observed as a native point defect after implantation, while the concentrations of all defect complexes (V_{Zn}+V_O, V_{Zn}+2V_O and 4V_{Zn}+V_O) increase as a result of the implantation and annealing processes.

Comparing all calculated weights of considered models presented in **Table 1**, the following scenario of the native point defect evolution could be proposed. The diffusion barrier for interstitial zinc atoms (Zn_{oct}) in ZnO is rather low, so migration of these atoms combined with a filling of some zinc vacancies could partially explain lower concentration of V_{Zn} in the implanted and annealed material. However, it can be concluded that the formation of V_{Zn} + V_O and 4V_{Zn} + V_O defect complexes is responsible for the disappearance of the V_{Zn} native point defect. As can be seen from the values given in **Table 1**, any similar reasoning cannot be made for the oxygen vacancy, as the concentration of V_O increases both in the form of isolated point defect and as a part of defect clusters as well. Therefore, it can be concluded that the Yb implantation and subsequent annealing processing leads to the formation of oxygen vacancies that appear in the implanted material not only as isolated point defects, but also as a part of V_{Zn} + V_O, V_{Zn} + 2V_O and 4V_{Zn} + V_O complexes. It also should be noted that while these complexes (except V_{Zn}+2V_O) are present in the virgin sample, their amount in the implanted material increases significantly.

The absence of isolated oxygen vacancies in the virgin sample is a quite interesting finding, as according to the performed XANES studies, all oxygen vacancies are attracted by V_{Zn} leading to formation of V_{Zn} + V_O donor-acceptor complexes. However, the surface sensitivity of the XANES method should be also considered. All the samples were exposed to ambient air before the experiment, which resulted in the oxygen diffusion into the subsurface region and the subsequent disappearance of oxygen vacancies. On the other hand, the Yb implantation process resulted in the formation of additional oxygen vacancy defects that cannot be annihilated by the diffusion of ambient air oxygen.

Yb M_5 edge supported by XPS investigations

Once more we would like to remind that only TEY data are reported here, which means that the results cannot be safely/reliably extended to the whole film.

Let us note that for all rare earth elements, excluding Yb, the peaks that correspond to $M_{4,5}$ edges are well defined and are clearly visible. In case of Yb^{3+}, only a single significant peak (M_5 edge) is shown in spectrum [23]. Such observation was explained in the literature [24,25] as follows. An absorption process involves the electronic excitation $3d^{10}4f^N \rightarrow 3d^94f^{N+1}$, where all other shells of the atom are either filled or empty. Consequently, the initial state for Yb^{3+} is $4f^{13}$. It has L = 3 and S = 1/2. The two possible values of J are 5/2 and 7/2 and the ground state is that with J = 7/2 according to Hund's rule. Due to spin-orbit coupling the $^4F_{5/2}$ state has an energy difference with the ground state of approximately 1.3 eV. After 3*d* absorption the final state is $3d^94f^{14}$, described by term symbols $^2D_{3/2}$ and $^2D_{5/2}$. Due to the spin-orbit coupling the energy difference between these two terms is 49 eV. However, in the X-ray absorption spectrum, just the $^2D_{5/2}$ line (corresponding to the M_5 edge) is present, since the $^2D_{3/2}$ term cannot be reached from the $^4F_{7/2}$ ground state because of the ΔJ selection rules. It is worth noticing that transitions to both final states are possible from the $^4F_{5/2}$ excited initial state, but that at room temperature very few atoms are in the excited state.

Consequently, **Figure 2** shows the Yb M_5-edge XANES spectra taken in TEY mode for ZnO:Yb films after annealing. Comparison to Yb_2O_3 powdered sample indicates that the main resonance at 1520.6 eV is associated to Yb^{3+}. The measurements for implanted samples were performed in consideration of polarization effect of synchrotron radiation (see details in the section concerning O *K* edge measurements). Crucial is the fact that there is a strong polarization dependence. The variation of the peak intensity represents the variation of the Yb^{3+} concentration along with polarization dependence in the proximity of the sample surface. The existence of a polarization dependence shown in **Figure 2a)** is intuitively clear if one looks at angular dependence of the *f* orbitals. Unexpected here is the inversion of the polarization relationships (compare **Figure 2 a)** vs **b)**) for a sample with a higher dose of Yb (this will be discussed further).

Conventional XPS studies do not reveal pronounce differences in the O 1s and Zn 2p photo-peaks for implanted/annealed samples, see **Figure 3a, b)**, so their general trend is shown. The O 1s peak can be deconvoluted by 3 constituent peaks. The peaks located at about 530.82 eV (marked by O_{LAT}), 531.40 eV (marked by O_{VAC}), and 532.68 eV (marked by ADS) are related to oxygen in a wurtzite ZnO lattice [26]; to oxygen vacancy defects [27]; and to the surface-adsorbed oxygen species of O^{2-}[28], respectively. Estimated binding energy of Zn $2p_{3/2}$ line is 1022.2 eV. Obtained value is close to one for ZnO [~1022 eV, 29]. The spin-orbit splitting for Zn $2p_{3/2}$ and Zn $2p_{1/2}$ is 23.1 eV which indicates that zinc atoms are in +2 oxidation state (Zn-O bonding) [30]. Next, **Figure 3c**) shows contour plot of Yb 4d line recorded after subsequent steps of sputter profiling analysis, 1 min per point, for selected sample. An example of Yb 4d line for as-received and sputtered by 1 min. shown in **Figure 3d**). The authors were interested in whether there are visible changes in the electronic structure around Yb along the sample

depth. In our previous work, where Si/Nb/Si system was investigated, it was shown that even under gentle sputtering regime, the depth profile changed significantly [31]. It was shown that significant mixing of silicon and niobium atoms took place, leading to the formation of a silicon-niobium solution. Presented here contour plot do not reveal strong mixing of implanted atom with the host matrix. Thus, the material studied in this work is stable during the applied Ar^+ sputtering. Further, XPS studies reported in **Figure 3c, d)** have shown that for the investigated samples ytterbium 4d levels show an extended multiple structure instead of a simple spin–orbit doublet of metallic ytterbium. Obtained data agree well with synchrotron XPS measurements for similar system [32,33]. Taking into account an influence of oxidation on the Yb 4*d* spectrum profile and similarity of spectrum profile examined in this work to the Yb_2O_3 (see **Fig. 2b** in [32]), we propose here that : i) the majority of ytterbium atoms are Yb^{3+}; ii) they are located in the interstitial positions and form near local range YbO_6 close to one in Yb_2O_3 and show an extended multiple structure indicating that electron of the 4*f* shell has been promoted to the valence level. Consequently, we assume that the inversion of the polarization dependence shown in **Figure 2** can be associated with a tilt of the oxygen pseudo octahedra or/and with their distortion. As is well known, trivalent rare earth (RE) ions usually have octahedral configuration. Thus, to minimize the energy, the local surrounding of RE ion in the ZnO host matrix is usually modified to approach the octahedral. The crystal field around RE centers is additionally modified during annealing, to attain the suitable symmetry allowing the intra-4*f* transitions [34-36]. As mentioned above, the preliminary studies based on XPS and the resonant photoemission spectroscopy (RPES) of ZnO:Yb [32,33] suggested that after annealing Yb ions are surrounded by six oxygen atoms forming a pseudo-octahedron structure YbO_6 with reduced symmetry instead of O_h. Thus, for instance, in the ytterbium oxide the Yb atoms occupy two "pseudo octahedral" sites with eight atoms in positions with three-fold inversion symmetry C3i, and 24 atoms in positions with two-fold symmetry C2 [37]. The symmetry modification towards the lower one could be the reason behind the activation of luminescence [36]. Thus, for an unambiguous interpretation of our assumptions, studies for the XAFS Yb L3 edge are necessary along with more detailed theoretical calculations.

Discussion

Generally, if an intrinsic defect is stable over a wide range of experimental conditions, it can be tricky to eliminate it, and it is likely to be present in samples. Vacancy clusters have been identified before in ZnO by PAS in ion implanted and then annealed samples [9,38,39], meaning that they typically result from non-equilibrium processes. Thermodynamically these clusters are unstable, but once formed they can be very difficult to remove due to large binding energy. In some cases, thermal treatments at about 800°C are required for their annihilation, but for instance in N-implanted samples, the clusters are stabilized somehow, and remain stable up to 1000°C [40]. In context of defect type influence on Photoluminescence (PL) signal in UV/visible region, Dong et al. [9] attribute the PL peak at 1.6 eV to isolated Zn vacancies or small $n(V_{Zn})$ groups ($n \leq 2$, and O vacancies may be present). It was argued that this peak shifts to 1.9-2.1 eV upon annealing, as more vacancies cluster together (including O

vacancies). However, let us note that PAS cannot distinguish between the isolated Zn vacancy, and small clusters $n(V_{Zn}–V_O)$ with $n \leq 2$ [6]. As a result of this, it has not been possible to unambiguously assign, e.g., luminescence resonance data to any single candidate. Thus, red luminescence (RL) has often been assigned to Zn vacancy related defects [9, 41-43]. While this is accepted by some authors, it is still not completely clear exactly what configurations are responsible for individual signals. For instance, using PL investigations instead of PAS, V_{Zn} has been identified previously as being responsible for the emission centered around 2.35 eV [44] what correspond to green emission. In any case, XAS results presented here indicate that after annealing of implanted by Yb ZnO films donor-acceptor complexes (and not isolated V_{Zn}) might be partially responsible for PL signal at about 590-653 nm region (i.e., the region that partially covers yellow and red emissions). PL spectra of investigated here films measured in the visible region were shown in Fig. 5 in [52]. Let us now continue with considerations of other defects. There are some reports claiming that the violet-blue emission is mainly associated to zinc interstitials (marked as Zn_{oct} in **Table 1**) inside ZnO band gap [45-50]. Whereas, the green emission is most likely associated with the damage on the oxygen sublattice. The prime candidates of point defects on the oxygen sublattice are V_O and O_i [43, 44, 51]. The obtained results shown in **Table 1** confirm that V_O located at least in the surface area of the annealed Yb implanted ZnO sample may be responsible for the green emission, while the model describing interstitial oxygen most likely was below the sensitivity limit of the technique used in this work or is absent. Let us focus the reader's attention to the fact that the authors of this work, at this stage, do not take into account the contribution of implanted ytterbium ions and its complexes with intrinsic point defects on the PL signal in visible region. The attention is drawn rather to the fact that the results obtained up to this point fit well into the relationship established in the literature between intrinsic defects and their complexes to PL signal in the visible region.

Analysis of presented data suggests that formed V_{Zn}-donor complexes will have an impact on the electrical properties of investigated here samples. V_{Zn} defects act as acceptors and increase resistance, while vacancy clusters remove isolated V_{Zn}, thereby decreasing resistance. Such an effect was observed previously in experiments with irradiation induced electrical isolation [53] and is true for the samples examined there. Thus, our Hall measurements point out that resistivity of annealed ZnO:Yb film with fluence 5e15 ions/cm^2 is about one order lower (10^{-1} Ω·cm) compared to the annealed one with fluence 5e14 ions/cm^2 (10^{-2} Ω·cm).

Conclusions

The polarization-depended XANES spectra of epitaxial ZnO (virgin and doped with Yb) thin films grown by ALD were obtained and analyzed. Anisotropic effects along film growth direction (c-axis) were observed. The orbital-resolved calculations of w-ZnO XANES spectrum provided by FEFF code for O *K* edge successfully reproduced these anisotropic effects shedding light on the responsible mechanisms. The used linear combination of theoretical models corresponded to selected point defects and their complexes confirmed the presence, along with isolated defects, of donor-acceptor complexes

in the samples under study. The analysis of the Yb M_5 edge of XANES spectra revealed that oxidation states of Yb in ZnO is 3+. Obtained result agree well with XPS and former RPES investigations. Yb M_5 XANES spectra also reveal anisotropic effect. The inversion of the polarization dependence for samples with different Yb fluences can be associated with a tilt of the oxygen pseudo octahedra or/and with their distortion. Analysis of presented data suggests that formed acceptor-donor complexes can have an impact on the electrical properties of samples investigated in this work. This suggestion confirmed by previous Hall measurements indicating that resistivity of annealed ZnO:Yb film with fluence 5e15 ions/cm^2 decreases by about one order compared to one with fluence 5e14 ions/cm^2.

Acknowledgements:
We acknowledge National Synchrotron Radiation Centre SOLARIS for provision of synchrotron radiation facilities, and we would like to thank the team of beamline "PEEM/XAS" for assistance. The work was partially supported by the Interdisciplinary Centre for Mathematical and Computational Modelling (ICM) at University of Warsaw, Poland, grant ID G59-20. The samples growth was co-financed by international project supported by the Polish Ministry of Science and Higher Education (3846/HZDR/2018/0) and Helmholtz-Zentrum Dresden-Rossendorf (17000941-ST). We would also like to thank Prof. M. Wierzbowska of Institute of High Pressure Physics of Polish Academy of Sciences, Warsaw, Poland for fruitful discussions.

References

[1] Z. Q. Chen, M. Maekawa, S. Yamamoto, A. Kawasuso, X. L. Yuan, T. Sekiguchi, R. Suzuki, and T. Ohdaira, Phys. Rev. B 69, 035210, (2004); https://doi.org/10.1103/PhysRevB.69.035210
[2] Z. Q. Chen, A. Kawasuso, Y. Xu, and H. Naramoto, Journal of Applied Physics 97, 013528 (2005); https://doi.org/10.1063/1.1821636
[3] N. Tiwari, S. Kumar, A. K. Ghosh, S. Chatterjee, S. N. Jha and D. Bhattacharyya, RSC Adv., 2017, 7, 56662–56675; https://doi.org/10.1039/C7RA10748J
[4] Z. Q. Chen, S. Yamamoto, M. Maekawa, and A. Kawasuso, Journal of Applied Physics 94, 4807 (2003); https://doi.org/10.1063/1.1609050
[5] Sreetama Dutta, Mahuya Chakrabarti, S. Chattopadhyay, and Debnarayan Jana, Journal of Applied Physics 98, 053513 (2005); https://doi.org/10.1063/1.2035308
[6] Ilja Makkonen, Esa Korhonen, Vera Prozheeva and Filip Tuomisto, Journal of Physics: Condensed Matter, Volume 28, Number 22 (2016), 224002; https://doi.org/10.1088/0953-8984/28/22/224002
[7] Tuomisto, F., Rauch, C., Wagner, M. R., Hoffmann, A., Eisermann, S., Meyer, B. K., Kilanski, L., Tarun, M. C., & McCluskey, M. D. Journal of Materials Research, 28(15), 1977-1983. (2013); https://doi.org/10.1557/jmr.2013.195
[8] Junhyeok Bang, Youg-Sung Kim, C. H. Park, F. Gao, and S. B. Zhang, Appl. Phys. Lett. 104, 252101 (2014); https://doi.org/10.1063/1.4884653
[9] Yufeng Dong, F. Tuomisto, B. G. Svensson, A. Yu. Kuznetsov, and Leonard J. Brillson, Phys. Rev. B 81, 081201(R); https://doi.org/10.1103/PhysRevB.81.081201
[10] E. Guziewicz, R. Ratajczak, M. Stachowicz, D. Snigurenko, T.A. Krajewski, C. Mieszczynski, K. Mazur, B.S. Witkowski, P. Dluzewski, K. Morawiec, A. Turos, Thin Solid Films, Volume 643, 2017, Pages 7-15; https://doi.org/10.1016/j.tsf.2017.08.014
[11] Guziewicz, E., Kobyakov, S., Ratajczak, R., Wierzbicka, A., Wozniak, W. and Kaminska, A. (2020), Optical Response of Epitaxial ZnO Films Grown by Atomic Layer Deposition and Coimplanted with Dy and Yb. Phys. Status Solidi B, 257: 1900513; https://doi.org/10.1002/pssb.201900513
[12]. F.A. Cotton, Chemical Applications of Group Theory (Willey, New York, 1971); https://doi.org/10.1002/bbpc.19720760217
[13] J-H Guo, L Vayssieres, C Persson, R Ahuja, B Johansson and J Nordgren. Journal of Physics: Condensed Matter, Volume 14, Number 28, 6969; http://dx.doi.org/10.1088/0953-8984/14/28/308
[14] I A Kowalik, E Guziewicz, M Godlewski and D Arvanitis, Journal of Physics: Conference Series 712 (2016) 012104; https://doi.org/10.1088/1742-6596/712/1/012104
[15] O. Bunau and Y. Joly J. Phys.: Condens. Matter 21, 345501 (2009); https://doi.org/10.1088/0953-8984/21/34/345501
[16] J. Stöhr, NEXAFS Spectroscopy (Springer, Berlin, 1992) ISBN: 978-3-662-02853-7; https://doi.org/10.1007/978-3-662-02853-7
[17] W.Gudat, PhD thesis (Hamburg University, 1974), International Report No. DESY F41-74/10.
[18] R.G. Jones and D.P. Woodruff, Surface Science, Volume 114, Issue 1, (1982), 38-46; https://doi.org/10.1016/0039-6028(82)90454-X
[19] Martens, G., Rabe, P., Schwentner, N. & Werner, A. (1978). J. Phys. C, 11, 3125–3133; https://doi.org/10.1088/0022-3719/11/14/032
[20] G. Martens et al., Phys. Stat. Sol. A, 55, 105 (1979); https://doi.org/10.1002/pssa.2210550110
[21] A. Janotti, C.G. Van de Walle, Phys. Rev. B 76, 165202 (2007); https://doi.org/10.1103/PhysRevB.76.165202
[22] Storn, R., Price, K. Journal of Global Optimization 11, 341–359 (1997). https://doi.org/10.1023/A:1008202821328
[23] Goedkoop, J.B. (Dec 1989). X-ray dichroism of rare earth materials. Available from INIS: http://inis.iaea.org/search/search.aspx?orig_q=RN:21039034

[24] de Groot, F. and A. Kotani, Core Level Spectroscopy of Solids. Advances in Condensed Matter Science. 2008. CRC Press; https://doi.org/10.1201/9781420008425
[25] B. T. Thole, G. van der Laan, J. C. Fuggle, G. A. Sawatzky, R. C. Karnatak, and J.-M. Esteva Phys. Rev. B 32, 5107 (1985); https://doi.org/10.1103/PhysRevB.32.5107
[26] S Pal et al 2018 J. Phys. D: Appl. Phys. 51 105107; https://doi.org/10.1088/1361-6463/aaa992
[27] Ming-Jie Zhao et al., Materials (Basel). 2020 Sep; 13(18): 3910; https://doi.org/10.3390/ma13183910
[28] Zhang, X. et al. Sci. Rep. 4, 4596 (2014); https://doi.org/10.1038/srep04596
[29] Wehner P.S., Mercer P.N., Apai G. J. Catal. 84, 244 (1983); https://doi.org/10.1016/0021-9517(83)90103-3
[30] Langer D.W., Vesely C.J., Phys. Rev. B 2, 4885 (1970); https://doi.org/10.1103/PhysRevB.2.4885
[31] I.N. Demchenko et al., Applied Surface Science Volume 399, 31 March 2017, Pages 32-40; https://doi.org/10.1016/j.apsusc.2016.12.028
[32] I. Demchenko , Y. Melikhov , P. Konstantynov , R. Ratajczak , A. Barcz , E. Guziewicz, Acta Physica Polonica A, Vol. 133 (2018); http://dx.doi.org/10.12693/APhysPolA.131.907
[33] I.N. Demchenko, R. Ratajczak, Y. Melikhov, P. Konstantynov, E. Guziewicz, Materials Science in Semiconductor Processing 91 (2019) 306–309; https://doi.org/10.1016/j.mssp.2018.11.037
[34] P. Kumar, V. Sharma, A. Sarwa, A. Kumar, Surbhi, R. Goyal, K. Sachdev, S. Annapoorni, K. Asokan, D. Kanjilal, RSC Adv. 6, 89242 (2016); https://doi.org/10.1039/C6RA17761A
[35] F.Benz, A.Gonser, R. Völker, T. Walther, J-T Mosebach, B. Schwanda, N. Mayer, G. Richter, H.P. Strunk, J. Lumin. Journal of Luminescence, Vol: 145, 855-858 (2014); https://doi.org/10.1016/j.jlumin.2013.09.014
[36] R. Anjana, M. K. Jayaraj, A. K. Yadav, S. N. Jha, and D. Bhattacharyya, Journal of Applied Physics 123, 153102 (2018); https://doi.org/10.1063/1.5022638
[37] Pandey et al. AIP Advances 3, 122123 (2013); https://doi.org/10.1063/1.4858421
[38] F. Tuomisto, K. Saarinen, D. C. Look, and G. C. Farlow, Phys. Rev. B, vol. 72, p. 085206 (2005); https://doi.org/10.1103/PhysRevB.72.085206
[39] Moe Børseth, T., Tuomisto, F., Christensen, J. S., Monakhov, E. V., Svensson, B. G., & Kuznetsov, A. Y. Physical Review B, 77(4), 1-6. [045204] (2008); https://doi.org/10.1103/PhysRevB.77.045204
[40] F. Tuomisto, C. Rauch, M. R. Wagner, A. Hoffmann, S. Eisermann, B. K. Meyer, L. Kilanski, M. C. Tarun, and M. D. McCluskey, “Nitrogen and vacancy clusters in zno,” Journal of Materials Research, vol. 28,
[41] L. Kappers, O. Gilliam, S. Evans, L. Halliburton, and N. Giles, Nuclear Instruments and Methods in Physics Research Section B: Beam Interactions with Materials and Atoms, vol. 266, no. 12–13, pp. 2953 – 2957, (2008); https://doi.org/10.1016/j.nimb.2008.03.146.
[42] Y. N. Chen, S. J. Xu, C. C. Zheng, J. Q. Ning, F. C. C. Ling, W. Anwand, G. Brauer, and W. Skorupa, Appl. Phys. Lett. 105, 041912 (2014); https://doi.org/10.1063/1.4892356
[43] K. E. Knutsen, A. Galeckas, A. Zubiaga, F. Tuomisto, G. C. Farlow, B. G. Svensson, and A. Yu. Kuznetsov, Phys. Rev. B 86, 121203 (2012); https://doi.org/10.1103/PhysRevB.86.121203
[44] T. M. Børseth, B. G. Svensson, and A. Yu. Kuznetsov, Appl. Phys. Lett. 89, 262112 (2006); https://doi.org/10.1063/1.2424641
[45] Ghosh A, Choudhary R.N.P, Journal of Applied Physics 105, 124906 (2009); https://doi.org/10.1063/1.3149786
[46] Yaoming Li, Linhua Xu, Xiangyin Li, Xingquan Shen, Ailing Wang, Applied Surface Science, Volume 256, Issue 14, (2010); https://doi.org/10.1016/j.apsusc.2010.02.044
[47] S.A.M Lima, F.A Sigoli, M Jafelicci Jr, M.R Davolos, International Journal of Inorganic Materials, Volume 3, Issue 7, (2001), 749-754; https://doi.org/10.1016/S1466-6049(01)00055-1
[48] Bixia Lin and Zhuxi Fu, Appl. Phys. Lett. 79, 943 (2001); https://doi.org/10.1063/1.1394173

[49] A. Zendehnam, M. Mirzaee, S. Miri, Applied Surface Science, Volume 270, (2013), 163-168; https://doi.org/10.1016/j.apsusc.2012.12.154
[50] Lim K, Abdul HMA, Shamsudin R, Al-Hardan NH, Mansor I, Chiu W, Materials 2016, 9(4), 300; https://doi.org/10.3390/ma9040300
[51] K. Vanheusden, C. H. Seager, W. L. Warren, D. R. Tallant, and J. A. Voigt, Appl. Phys. Lett. 68, 403 (1996); https://doi.org/10.1063/1.116699
[52] Ratajczak, R.; Mieszczynski, C.; Prucnal, S.; Krajewski, T. A.; Guziewicz, E.; Wozniak, W.; Kopalko, K.; Heller, R.; Akhmadaliev, S. Applied Surface Science 521(2020), 146421; https://doi.org/10.1016/j.apsusc.2020.146421
[53] A. Zubiaga et al., Phys. Rev. B 78, 035125 2008; https://doi.org/10.1103/PhysRevB.78.035125

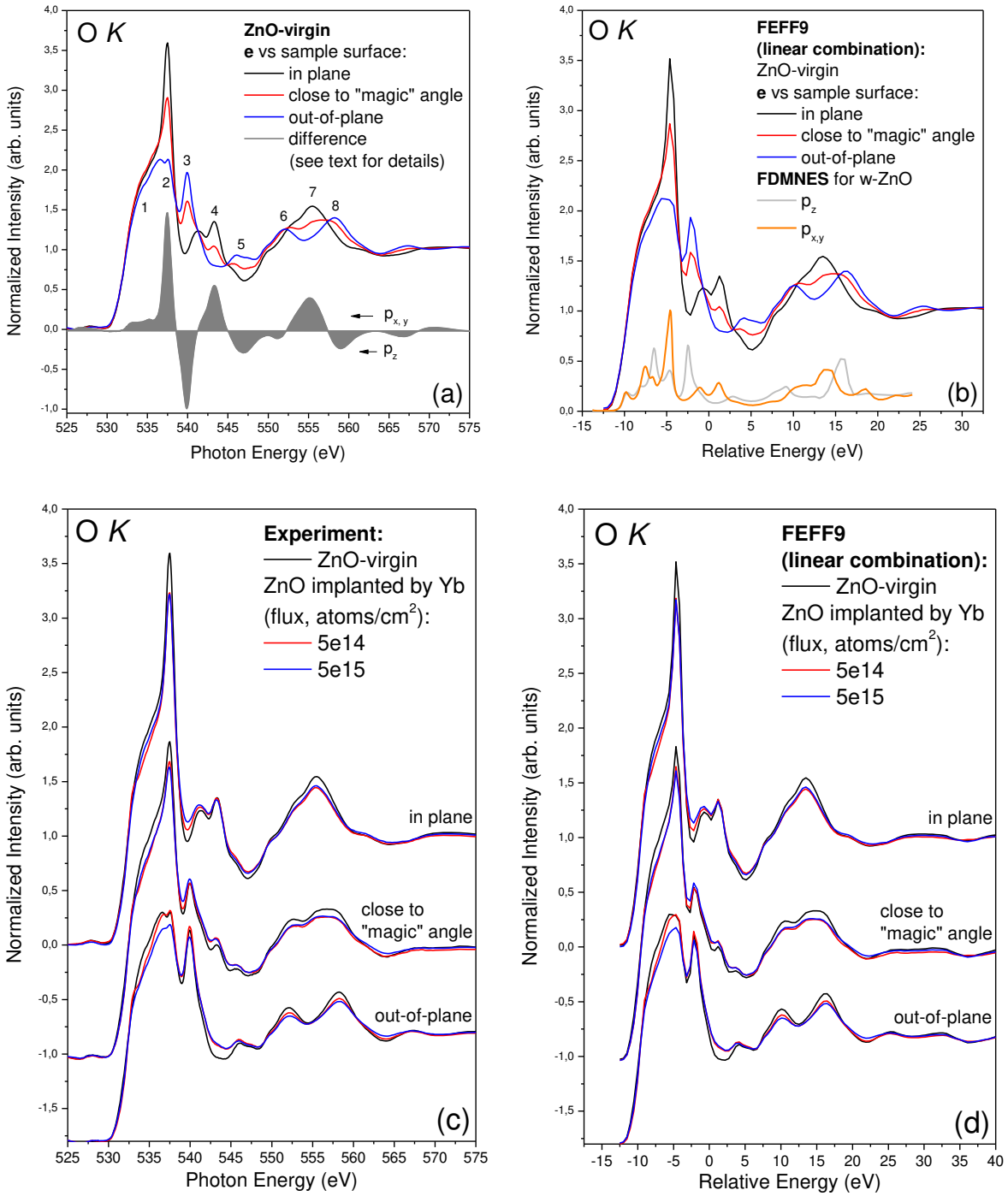

Figure 1. (a,c) Comparison of O 1s XANES spectra of a reference ZnO film and of ZnO:Yb films with different doses of Yb (5e14 and 5e15 atoms/cm²). All samples are after RTA. (b,d) O K XANES spectra obtained by linear combination of selected theoretical models calculated by FEFF code (see text for details) for different polarization geometry. (For interpretation of the references to color in this figure legend, the reader is referred to the Web version of this article.)

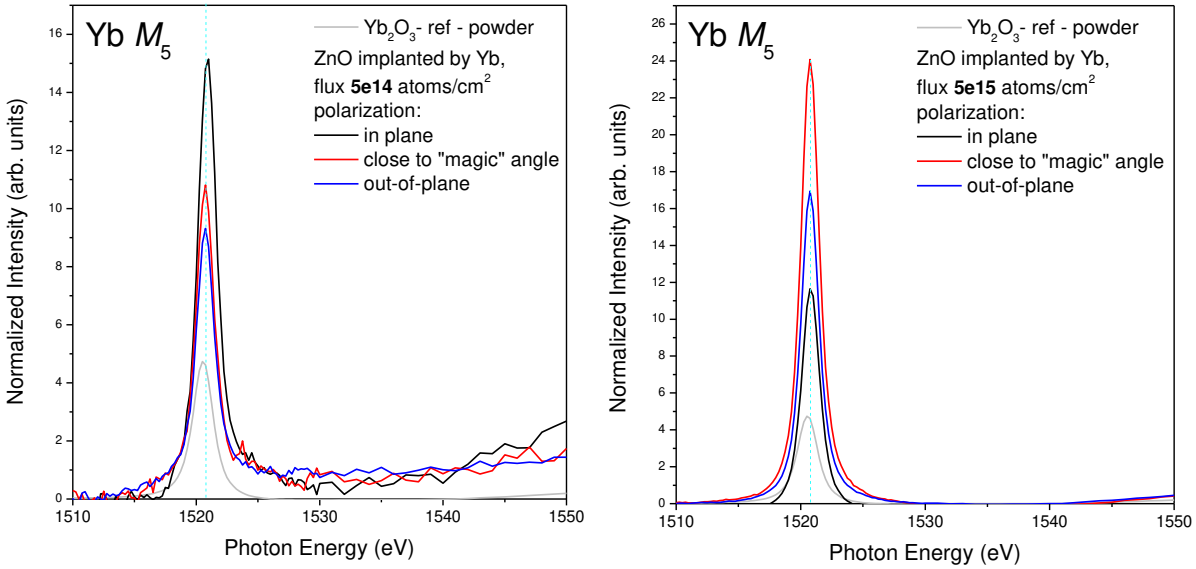

Figure 2. (a) Comparison of Yb M5 XANES (TEY) of ZnO:Yb films spectra of a reference ZnO film and of ZnO films with different doses of Yb (5e14 and 5e15 atoms/cm^2 after RTA). (For interpretation of the references to color in this figure legend, the reader is referred to the Web version of this article.)

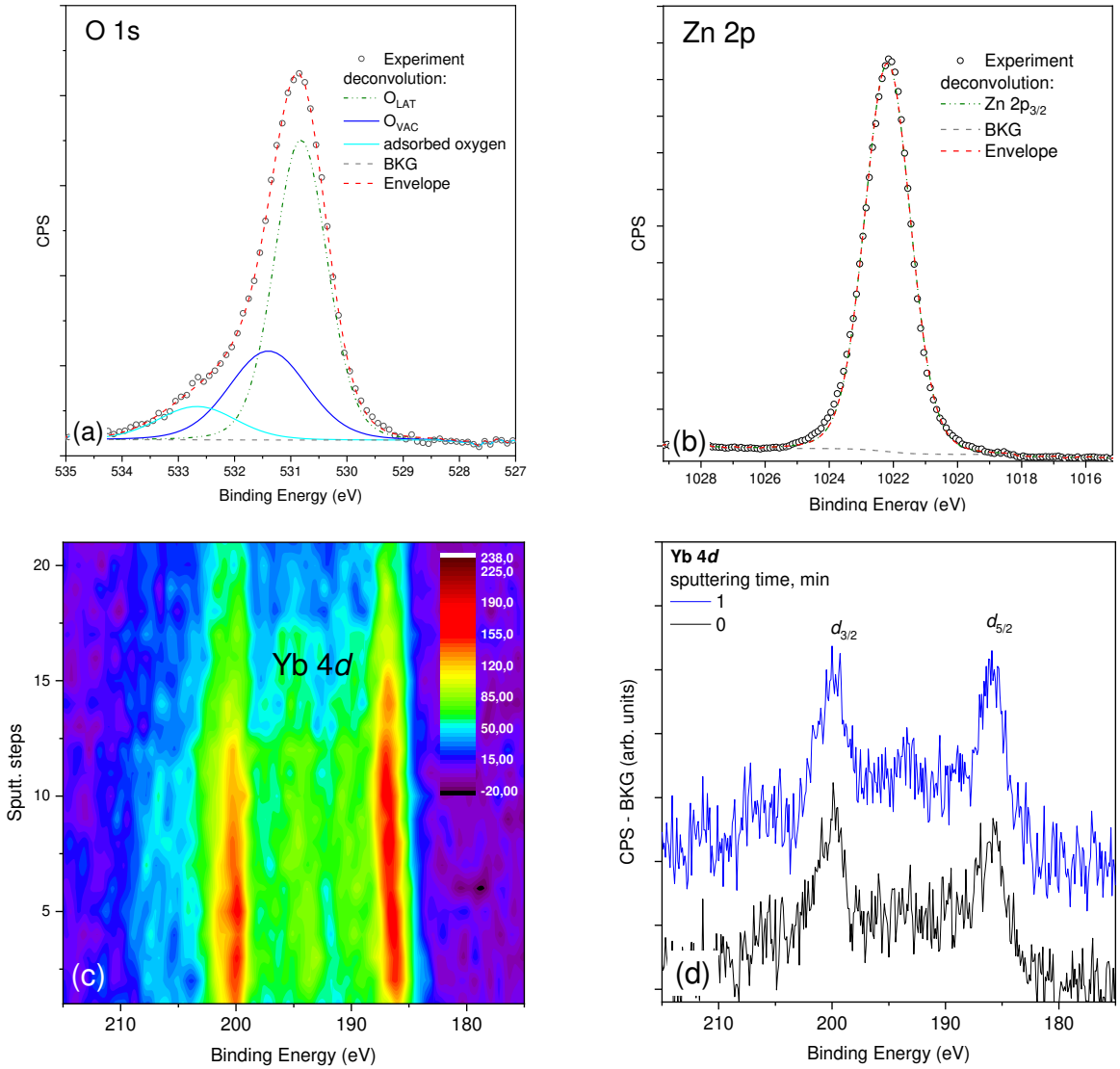

Figure 3. Experimental XPS results for the ZnO:Yb sample: O 1s (a); Zn 2p (b) peaks; Yb 4d contour plot (c) and (d) spectra for selected sputtering minutes.

Table 1. Results of linear combination of theoretical spectra obtained using the *differential evolution* routine (see text for details)

Sample	**model**	**weight**
ZnO	ZnO + $1V_{Zn}$ (*out-of-plane*)	0.28
R_f*=0.027,* σ^2*=0.035*	ZnO + $1V_O$	0.00
	ZnO + $1Zn_{oct}$	0.38
	ZnO + ($1V_{Zn}$+$1V_O$ – complex)	0.26
	ZnO + ($1V_{Zn}$+$2V_O$ – complex)	0.00
	ZnO+($4V_{Zn}$+$1V_O$ – complex)	0.07
5e14	ZnO + $1V_{Zn}$ (*out-of-plane*)	0.00
R_f *=0.022,* σ^2*=0.028*	ZnO + $1V_O$	0.20
	ZnO + $1Zn_{oct}$	0.34
	ZnO + ($1V_{Zn}$+$1V_O$ – complex)	0.31
	ZnO + ($1V_{Zn}$+$2V_O$ – complex)	0.00
	ZnO + ($4V_{Zn}$+$1V_O$ – complex)	0.15
5e15	ZnO + $1V_{Zn}$ (*out-of-plane*)	0.00
R_f *=0.018,* σ^2*=0.022*	ZnO + $1V_O$	0.15
	ZnO + $1Zn_{oct}$	0.31
	ZnO + ($1V_{Zn}$+$1V_O$ – complex)	0.33
	ZnO + ($1V_{Zn}$+$2V_O$ – complex)	0.08
	ZnO + ($4V_{Zn}$+$1V_O$ – complex)	0.13